Journal of Power Sources 634 (2025) 236502

Contents lists available at ScienceDirect

Journal of Power Sources

journal homepage: www.elsevier.com/locate/jpowsour

The role of Al substitution in Na_3AlH_6 hydrides: Structural and thermodynamic insights for hydrogen storage technologies

Abdelmajid Assila [a,*], Ikram Belkoufa [a], Seddiq Sebbahi [a,b], Amine Alaoui-Belghiti [a], El-kebir Hlil [c], Mouhaydine Tlemçani [d,e], Abdelowahed Hajjaji [a], Said laasri [a,f,**]

[a] Chouaib Doukkali University of El Jadida, National School of Applied Sciences, Energy Science Engineering Lab, El Jadida, Morocco
[b] Research Institute for Solar Energy and New Energies (IRESEN), Morocco
[c] Univ. Grenoble Alpes, CNRS, Grenoble INP, Institut N'eel, 38000, Grenoble, France
[d] Department of Mechatronics Engineering, School of Science and Technology, Universidade de Evora, Colégio Luis Antonio Verney, Rua Romao Ramalho, N° 59, 7000–671, Evora, Portugal
[e] Instrumentation and Control Laboratory, Institute of Earth Sciences, Universidade de Evora, Colégio Luis Antonio Verney, Rua Romao Ramalho, N° 59, 7000–671, Evora, Portugal
[f] Polydisciplinary Faculty of Sidi Bennour, Chouaib Doukkali University, El Jadida, Morocco

HIGHLIGHTS

- Development of the thermodynamic properties of the hydride Na_3AlH_6.
- Substituting aluminum with Be, Si, and Fe enhances Na_3AlH_6 for hydrogen storage.
- The criteria imposed by the DOE were validated during this work.
- Optimization of the storage capacity of Na_3AlH_6 hydride.

ARTICLE INFO

Keywords:
Hydrogen storage
Hydride
Na_3AlH_6
Thermodynamic properties
DFT

ABSTRACT

In this work, the structural, thermodynamic, and electronic properties, as well as the diffusion kinetics and volumetric and gravimetric capacities of sodium and aluminum hydride Na_3AlH_6, were evaluated and enhanced by substituting the aluminum element with Be ($Na_3Al_{1-x}BexH_6$), Si ($Na_3Al_{1-x}Si_xH_6$), and Fe ($Na_3Al_{1-x}Fe_xH_6$) with x = 0.25 and x = 0.5. All calculations were performed according to density functional theory (DFT), using the generalized gradient approximation (GGA) developed by Perdew, Burke, and Ernzerhof for solids (PBEsol). The results show an improvement in the thermodynamic properties. For instance, the formation enthalpy decreased from −82.25 kJ/mol.H_2 for the unsubstituted hydride Na_3AlH_6 to −34.24 kJ/mol.H_2 for ($Na_3Al_{0.75}Be_{0.25}H_6$) and −35.02 kJ/mol.$H_2$ for ($Na_3Al_{0.5}Si_{0.5}H_6$), values that closely align with those suggested by the U.S. Department of Energy (DOE). The decomposition temperature (T_d) dropped from 632.76 K for the unsubstituted hydride Na_3AlH_6 to 392.21 K for ($Na_3Al_{0.5}Fe_{0.5}H_6$), corresponding to the operational temperature range of hydrogen fuel cells (PEM) from 289 to 393 K. Furthermore, the gravimetric capacity of hydrogen increased from 5.93 wt% for the unsubstituted hydride Na_3AlH_6 to 6.40 wt% for $Na_3Al_{0.5}Be_{0.5}H_6$, in line with the DOE's recommended value of 6 wt%. Analysis of the density of states of Na_3AlH_6 revealed that the bandgap is 2.98 eV, indicating that the hydride Na_3AlH_6 is insulating. The activation energy of hydride Na_3AlH_6 varies between 0.8 and 3.05 eV.

1. Introduction

The current state of energy worldwide faces a major challenge: fossil fuels, such as oil, natural gas, and coal, will be depleted in the coming years, according to the U.S. Energy Information Administration (EIA) [1–4]. For instance, the estimated global reserves of oil and natural gas are about 50 years, while coal reserves are approximately 156 years [5, 6]. On the other hand, according to the Intergovernmental Panel on

* Corresponding author.
** Corresponding author. Chouaib Doukkali University of El Jadida, National School of Applied Sciences, Energy Science Engineering Lab, El Jadida, Morocco.
E-mail addresses: assila.a@ucd.ac.ma (A. Assila), laasrisaid@yahoo.fr (S. laasri).

https://doi.org/10.1016/j.jpowsour.2025.236502
Received 24 December 2024; Received in revised form 29 January 2025; Accepted 9 February 2025
Available online 13 February 2025

Climate Change (IPCC), global temperatures have risen by about 1.5 °C since the industrial revolution, between 1980 and 1999 [7]. The increase in temperature presents a threat to countries with coastal areas, raising the risk of the disappearance of certain islands and vulnerable regions [8]. If this increase continues along the same trends, a rise of up to 2 °C could be reached by the end of the century [9]. In this context, the Paris Conference (COP21) aims to limit global warming to between 1.5 and 2 °C above pre-industrial levels [8,9]. To reach this goal, it is essential to explore alternative energy sources that are less polluting and more abundant on Earth. Among the solutions identified so far are renewable energies such as solar, wind, hydroelectric, biomass, and marine energy [10]. However, these types of energy suffer from limitations related to their availability under all conditions, For example, marine energy cannot function if there are no waves [11].

In recent years, we have developed another type of energy: hydrogen-based energy, which is becoming a trend both now and in the future [12–17]. This is due to its sustainability and high energy content, as it has an energy density of 142 MJ/kg, approximately three times that of fossil resources [18,19]. Additionally, the conventional way of producing hydrogen through electrolysis of water without harmful greenhouse gas emissions is an another attractive advantage [8,9,20,21]. However, this new type of energy faces a major challenge in storage [22,23].

Many experts believe that storing hydrogen in the form of hydrides is safer than storing it in high-pressure cylinders, which require nearly 700 bars to contain 30 kg of hydrogen per cubic meter [18,24,25]. This poses a threat both for the storage and use of hydrogen. While liquid hydrogen storage offers an energy density of 8.4 MJ/L, higher than that of gaseous hydrogen at 4.4 MJ/L, it represents a significant challenge due to cooling and compression processes that result in nearly 30 % loss of stored energy in liquid hydrogen. Due to safety concerns associated with the hydrogenation process and the potential to reuse hydrides after discharge, solid storage remains one of the most sought-after methods in hydrogen storage [20,26–32]. However, one issue to address in solid storage is meeting certain criteria. If these hydrides do not meet the requirements set by the U.S. Department of Energy (DOE), they cannot be used as energy storage systems. Among these criteria, the formation enthalpy must be equal to −40 kJ/mol.H_2, the temperature must be between 289 and 393 K, and the gravimetric capacity must exceed 6 wt % [33–35]. Among the commonly developed hydrides in recent years are magnesium-based hydrides such as MgH_2 [23,36], Mg_2CoH_5 [37,38] and Mg_2NiH_4 [10], as well as complex hydrides like lithium borohydride, $LiBH_4$ [20,39], Sodium aluminum hydride, $NaAlH_4$ [40–43].

To broaden and enrich the research field on materials suitable for hydrogen storage, we have chosen sodium aluminum hydride, Na_3AlH_6, due to its hydrogen content and the competitive cost of aluminum and sodium in the market [26,44–48]. Additionally, Na_3AlH_6 has an activation energy of 0.62 eV, indicating that the hydrogenation process is relatively easy to achieve [49]. Furthermore, the storage capacity of sodium aluminum hydride is 5.5 wt% [47], which is close to the value suggested by the U.S. Department of Energy set at 6 wt%. However, its experimental formation enthalpy is −89 kJ/mol.H_2, and its decomposition temperature is 268 °C factors that require improvement [50]. Moreover, the strong bond between the Na^+ ions and $[AlH_6]^{3-}$ makes this hydride more stable, which complicates the release of hydrogen under ambient temperature and pressure conditions. This characteristic limits the large-scale use of this hydride, particularly in transport applications, which require safety guarantees. Studies have been conducted to improve the storage capacity of Na_3AlH_6, using $TiCl_3$ and Ti $(OBu)_4$ to dope Na_3AlH_6 [26]. This method showed an increase in storage capacity, but this was observed at temperatures ranging from 443.15 K to 543.15 K and under pressures ranging from 4.2 MPa to 6 MPa [27].

In this work, in order to optimize the thermodynamic properties and storage capacity of Na_3AlH_6 hydride, the aluminum element was replaced with three elements: Be (alkaline earth metal), Si (metalloid), and Fe (transition metal), at concentrations of 25 % and 50 %. The reason for choosing these elements was to examine the effect of various types of elements rather than just one. Additionally, these elements exhibit different characteristics, such as their valence electron counts: Be ($2s^2$), Si ($3s^2$ $3p^2$), and Fe ($3d^6$ $4s^2$) the electronic properties will be explained in Fig. 7. They also differ in atomic radii, molar masses, and electronegativity. These differences could lead to an increase in gravimetric capacity as well as improvements in formation enthalpy and decomposition temperature. To the authors' knowledge, the substitution of aluminum with Be, Si, and Fe has not been previously studied in the literature to enhance the thermodynamic properties or hydrogen storage capacity of Na_3AlH_6 hydride. Therefore, the results obtained in this work could guide future research on hydrogen storage in Na_3AlH_6 hydride, as well as studies that may utilize these hydrides in commercial applications for hydrogen fuel cells (PEM) [51].

2. Computational methodology

The calculations performed in this work are based on density functional theory (DFT) and utilize the Cambridge Serial Total Energy Package (CASTEP) computational code [52]. The generalized gradient approximation (GGA) developed by Perdew, Burke, and Ernzerhof for solids (PBE_{sol}) is used as the approximation for all calculations conducted [53]. An ultrasoft pseudopotential is applied with a cutoff energy of 410 eV, and the K points are defined at 6 × 5 × 3. The convergence energy is set to 5×10^{-7} eV, with an energy of 5×10^{-6} eV/atom. The maximum allowed force is 0.01 eV/Å, the maximum stress is 0.02 GPa, and the maximum displacement is 5×10^{-4} Å. The conventional cell of the Na_3AlH_6 system, belonging to space group P21/c (No. 14), consists of 12 hydrogen atoms, 6 sodium atoms, and 2 aluminum atoms [54]. Their positions are represented in Table 1.

3. Results and discussion

3.1. Structural Properties of Na_3AlH_6 and $Na_3Al_{1-x}M_xH_6$ (M = Be, Si, and Fe) (x = 0.25 and 0.5)

Before proceeding with the substitution of the aluminum (Al) element in sodium-aluminum hydride Na_3AlH_6 with other elements such as beryllium (Be), silicon (Si), and iron (Fe), it is essential to first optimize the structural parameters and the volume of the unit cell of Na_3AlH_6. This optimization enables the determination of the most accurate values for the crystalline structure of the hydride, ensuring that

Table 1
Fractional coordinates of atoms (u,v and w) of system Na_3AlH_6.

Element	Atom number	Fractional coordinates of atoms		
		u	v	w
H	1	0.224085	0.767069	1.063608
H	2	0.684627	0.830787	1.456388
H	3	0.883784	0.952070	1.283770
H	4	−0.224085	1.267069	−0.563608
H	5	−0.684627	1.330787	−0.956388
H	6	−0.883784	1.452070	−0.783770
H	7	−0.224085	−0.767069	−1.063608
H	8	−0.684627	−0.830787	−1.456388
H	9	−0.883784	−0.952070	−1.283770
H	10	0.224085	−0.267069	1.563608
H	11	0.684627	−0.330787	1.956388
H	12	0.883784	−0.452070	1.783770
Na	1	0.735274	0.953076	0.746054
Na	2	−0.735274	1.453076	−0.246054
Na	3	−0.735274	−0.953076	−0.746054
Na	4	0.735274	−0.453076	1.246054
Na	5	0.500000	0.000000	1.000000
Na	6	−0.500000	0.500000	−0.500000
Al	1	0.000000	0.000000	0.500000
Al	2	0.000000	0.500000	0.000000

the results are consistent with both experimental and theoretical data. The Na_3AlH_6 system (space group P21/c No. 14) evaluated in this work was reported by the official site (Materials Project) in 2014 with the following lattice parameters: a = 5.543 Å, b = 5.346 Å, and c = 9.384 Å [54]. These lattice parameters closely resemble the results obtained in this study, based on the GGA-PBEsol approximation, which yields a = 5.32 Å, b = 5.25 Å, and c = 9.34 Å, resulting in a volume of 260.86 $Å^3$. The results obtained during this work are summarized in Table 2.

Once this optimization is completed, the aluminum (Al) element in the Na_3AlH_6 structure will be substituted with 25 % and 50 % of Be, Si, and Fe (Fig. 1). The results show that the substitution led to a significant increase or decrease in volume. Specifically, the volume increases by almost half when the substitution is at 25 %, while with a 50 % substitution, the volume experiences a slight decrease. This variation can be explained by the fact that lower concentrations of substitutes create a repulsive force between the substituting atoms and the main atoms of the Na_3AlH_6 hydride. In contrast, higher concentrations of substituents may reduce the repulsive forces and increase the attractive forces between the atoms, resulting in a slight decrease in volume.

3.2. Volumetric and gravimetric capacity

To continue our study and gain a deeper understanding of the impact of the substitutions made on hydrogen storage, it is essential to examine the volumetric and gravimetric capacity of Na_3AlH_6 as well as $Na_3Al_{1-x}M_xH_6$ (where M = Be, Si, and Fe) for values of x equal to 0.25 and 0.5. The equations used to calculate the volumetric capacity (Equation (1)) and the gravimetric capacity (Equation (2)) are as follows [55]:

$$\rho_{Vol} = \frac{nM_H}{N_A V} \quad (1)$$

$$C_g = \frac{nM_H}{nM_H + 3M_{Na} + (1-x)M_{Al} + xM_M} \quad (2)$$

Where n is the number of hydrogen atoms in the unit cell, M_H is the molar mass of hydrogen, N_A is Avogadro's number, V is the volume of the unit cell, M_{Na} is the molar mass of sodium, M_{Al} is the molar mass of aluminum, M_M is the molar mass of the substituent (M = Be, Si, and Fe), and x is the percentage of substitution.

The results obtained are presented in Fig. 2 and show that a 25 % substitution with these elements reduced the volumetric capacity of Na_3AlH_6 from 36.6 g.H_2/L to approximately 20 g.H_2/L. In contrast, a 50 % substitution led to an increase in volumetric capacity, reaching up to 47.2 g.H_2/L for the iron element, which is greater than the minimum value of 40 g.H_2/L proposed by the DOE, this increase is due to the volume reduction of the substituted hydrides ($Na_3Al_{1-x}M_xH_6$) [33,34]. This variation can be explained by the repulsive or attractive forces created between the substituting elements and the main atoms of the Na_3AlH_6 hydride. At low concentrations of substitutes, repulsive forces may dominate, thereby reducing the volumetric capacity. Conversely, at higher concentrations, attractive forces may become more significant, resulting in an increase in volumetric capacity. These observations are crucial for understanding how different substitutions influence the properties of the material and for integrating these forces into the manufacturing of hydride in future research.

Table 2
Lattice Parameters and Volume of Na_3AlH_6 and $Na_3Al_{1-x}M_xH_6$ (M = Be, Si, and Fe; x = 0.25 and 0.5).

Structure	Lattice parameter (Å)			Volume ($Å^3$)
	a	b	c	
Na_3AlH_6	5.32	5.25	9.34	260.86
$Na_3Al_{0,75}Be_{0,25}H_6$	5.27	7.63	10.94	439.90
$Na_3Al_{0,75}Si_{0,25}H_6$	5.38	7.71	11.09	460.01
$Na_3Al_{0,75}Fe_{0,25}H_6$	5.31	7.61	10.84	438.03
$Na_3Al_{0,5}Be_{0,5}H_6$	5.26	5.40	7.55	214.45
$Na_3Al_{0,5}Si_{0,5}H_6$	5.39	5.59	7.75	233.51
$Na_3Al_{0,5}Fe_{0,5}H_6$	5.30	5.29	7.58	212.52

On the other hand, the gravimetric capacity of Na_3AlH_6 hydride is 5.93 wt%, making it an interesting candidate for hydrogen storage. The results are illustrated in Fig. 3, where the purple dotted line corresponds to the minimum capacity of 6 wt% proposed by the DOE [33,34,55]. This capacity was optimized with the substitution of aluminum by beryllium (Be), it reaches 6.06 wt% for a 25 % substitution rate of Be ($Na_3Al_{0.75}Be_{0.25}H_6$), and 6.40 wt% for a 50 % substitution rate of Be ($Na_3Al_{0.5}Be_{0.5}H_6$). These results align with the 6 wt% value proposed by the U.S. Department of Energy (DOE). In contrast, a slight decrease in gravimetric capacity is observed when aluminum is substituted with 25 % and 50 % of silicon (Si) ($Na_3Al_{0.75}Si_{0.25}H_6$ and $Na_3Al_{0.5}Si_{0.5}H_6$) or iron (Fe) ($Na_3Al_{0.75}Fe_{0.25}H_6$ and $Na_3Al_{0.5}Fe_{0.5}H_6$), with capacities ranging from 5.12 wt% to 5.81 wt%. However, these values remain close to those of the DOE [33,34,55]. The increase in gravimetric capacity with beryllium substitution, as well as the decrease observed with silicon and iron, can be explained by the fact that beryllium has a lower molar mass compared to the other substituting elements.

3.3. Thermodynamic Properties and hydrogenation kinetics

3.3.1. Activation energy

The activation energy is the energy required for a hydrogen atom to move from one site to another. If this energy is very low, the hydrogenation process is likely favored, conversely, if the energy is high, the process becomes more complex [10,39,56]. This quantity is therefore essential for understanding the kinetics of hydrogenation of Na_3AlH_6 hydride. To calculate this energy, it is necessary to know the energy of the Na_3AlH_6 system in all configurations where the hydrogen atom can exist. Thus, the activation energy is defined as the difference between the energy of the final state and that of the initial state. In Fig. 4, the activation energy is first calculated during the migration of the hydrogen atom to the first nearest neighbor site, and then during its migration to the second nearest neighbor site.

The results obtained show that the energy required for a hydrogen atom to move to the first nearest neighbor site is 0.8 eV, which is very close to the experimental value of 0.62 eV [49]. This activation energy value indicates that the diffusion of the hydrogen atom to the first site is feasible, leading us to conclude that Na_3AlH_6 hydride is promising for hydrogen storage applications. In contrast, the migration of the hydrogen atom from the first site to the second site requires an activation energy of 3.05 eV. This clearly indicates that the first migration of the hydrogen atom to the nearest neighbor site is much more favorable than the second migration. This difference in activation energy during the migration of the hydrogen atom, whether to the first or second site, can be attributed to several factors, such as the distance between the sites and the attractive or repulsive forces that influence this migration [20,56]. This means that Na_3AlH_6 has a higher stability, but it is necessary to reduce it to make it more suitable for hydrogen storage applications, which is the goal of the substitution.

3.3.2. Enthalpy of formation

The formation enthalpy factor ΔH is essential for determining suitable materials for hydrogen storage [23,39,57]. According to the U.S. Department of Energy (DOE), a material selected for hydrogen storage must have an enthalpy of −40 kJ/mol.H_2. If this enthalpy is greater than −40 kJ/mol.H_2, the hydride is considered thermodynamically unstable; conversely, if it is lower, the hydride is deemed more thermodynamically stable [20,56]. This enthalpy is generally defined as the difference between the total energy of the products and that of the reactants. In the case of Na_3AlH_6 hydride, the formation equation we use is as follows:

$$3Na + Al + 3H_2 \rightarrow Na_3AlH_6 \quad (3)$$

On the other hand, the formation equations used for the substitution

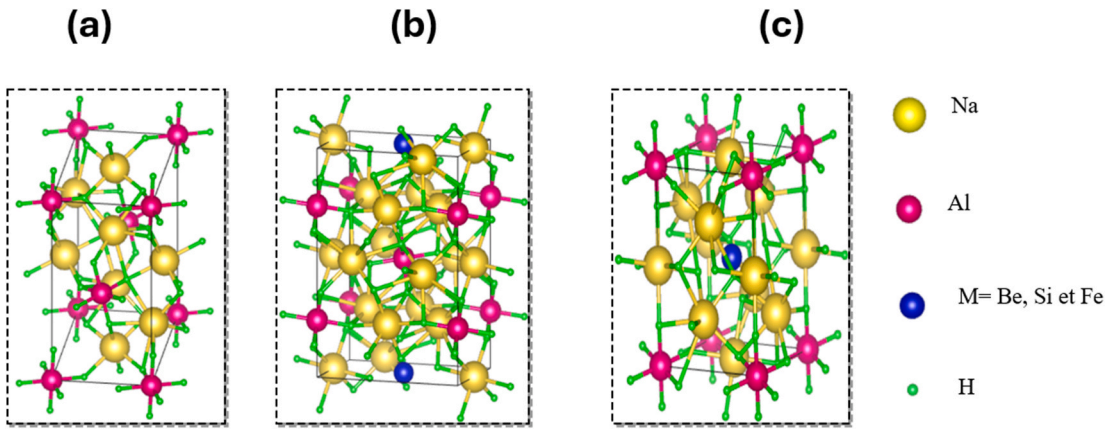

Fig. 1. Schematic representation of Na_3AlH_6 (a), $Na_3Al_{0.75}M_{0.25}H_6$ (b), and $Na_3Al_{0.5}M_{0.5}H_6$ (c) with (M = Be, Si, and Fe).

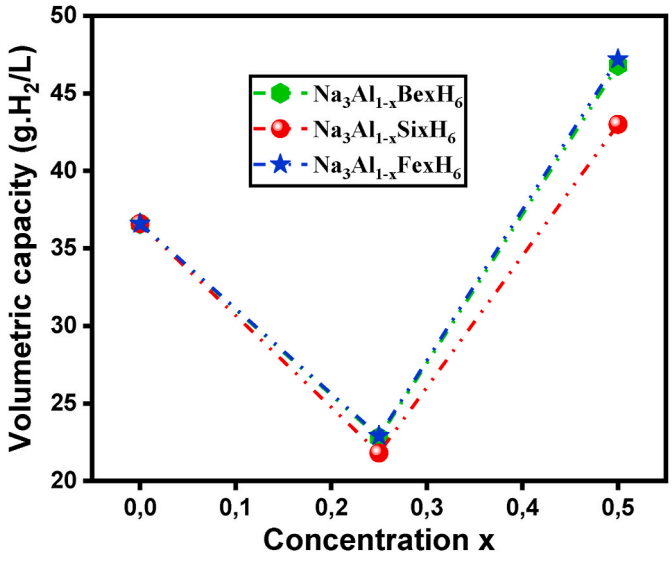

Fig. 2. Volumetric Capacity of Na_3AlH_6 and $Na_3Al_{1-x}M_xH_6$ (M = Be, Si, and Fe; x = 0.25 and 0.5).

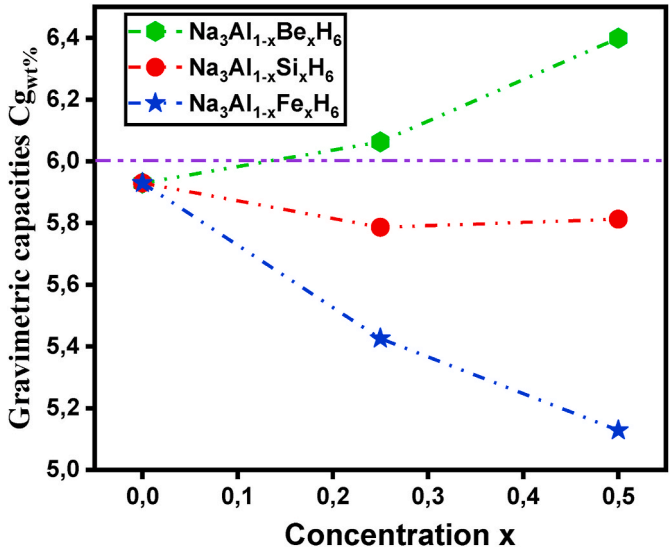

Fig. 3. Gravimetric Capacity of Na_3AlH_6 and $Na_3Al_{1-x}M_xH_6$ (M = Be, Si, and Fe; x = 0.25 and 0.5).

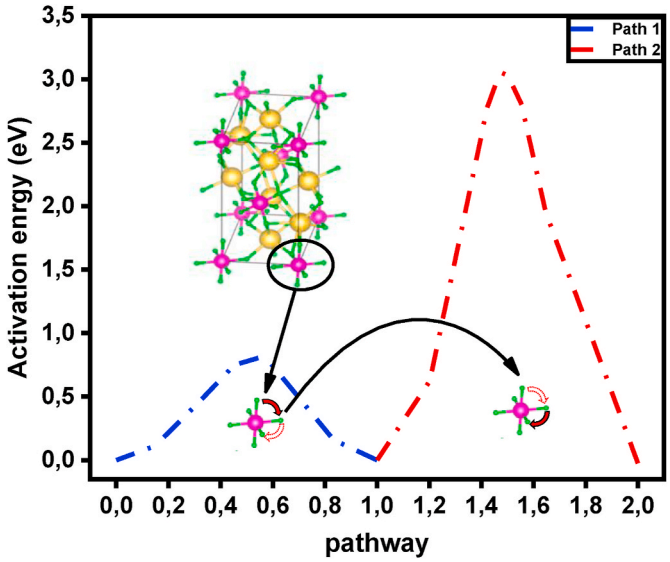

Fig. 4. Activation Energy of Na_3AlH_6 during the transition of the atom to the first nearest neighbor site and the second nearest neighbor site.

with 25 % and 50 % of beryllium (Be), silicon (Si), and iron (Fe) are as follows:

$$3Na + Al_{0.75}M_{0.25} + 3H_2 \rightarrow Na_3Al_{0.75}M_{0.25}H_6 \quad (4)$$

$$3Na + Al_{0.5}M_{0.5} + 3H_2 \rightarrow Na_3Al_{0.5}M_{0.5}H_6 \quad (5)$$

While the formation enthalpy is calculated by: for the Na_3AlH_6 hydride (Equation (6)), $Na_3Al_{0.75}M_{0.25}H_6$ (Equation (7)), and $Na_3Al_{0.5}M_{0.5}H_6$ (Equation (8)).

$$\Delta H = E_{tot}(Na_3AlH_6) - 3E_{tot}(Na) - E_{tot}(Al) - 3E_{tot}(H_2) \quad (6)$$

$$\Delta H = E_{tot}(Na_3Al_{0.75}M_{0.25}H_6) - 3E_{tot}(Na) - E_{tot}(Al_{0.75}M_{0.25}) - 3E_{tot}(H_2) \quad (7)$$

$$\Delta H = E_{tot}(Na_3Al_{0.5}M_{0.5}H_6) - 3E_{tot}(Na) - E_{tot}(Al_{0.5}M_{0.5}) - 3E_{tot}(H_2) \quad (8)$$

Based on Equation (6), the formation enthalpy of Na_3AlH_6 hydride is equal to −82.25 kJ/mol.H_2, indicating that Na_3AlH_6 has a very high thermodynamic stability. This result is in good agreement with the experimental results presented in Table 3:

However, this enthalpy needs to be developed to reach or approach the target value of −40 kJ/mol.H_2, which is considered a benchmark according to the U.S. Department of Energy (DOE) [33,34]. To reduce

Table 3
Formation enthalpy of the Na_3AlH_6 hydride.

Compound	Enthalpy of formation ΔH (kJ/mol.H_2)
Na_3AlH_6	−82.25 (This work) −89 [50] −69.7 [58] −69.6 [59]

the stability of the Na_3AlH_6 system, the aluminum element will be replaced by beryllium ($Na_3Al_{1-x}Be_xH_6$), silicon ($Na_3Al_{1-x}Si_xH_6$), and iron ($Na_3Al_{1-x}Fe_xH_6$) with x = 0.25 and x = 0.75. The results obtained using Equations (7) and (8) show that these substitutions can lead to a significant improvement in formation enthalpy, as illustrated in Fig. 4, where the blue dotted line corresponds to the enthalpy suggested by the DOE.

Fig. 5 shows that a 25 % insertion of Be into the aluminum of Na_3AlH_6 hydride reduces the formation enthalpy to −34.24 kJ/mol.H_2, which is very close to the −40 kJ/mol.H_2 value set by the DOE. Furthermore, a 50 % insertion of Be into the aluminum of Na_3AlH_6 decreases the enthalpy to 12.31 kJ/mol.H_2, indicating that the material would be thermodynamically unstable. In this context, we note that an increase in concentration leads to a linear decrease in formation enthalpy, and a 20 % percentage of (Be) could bring the enthalpy down to −40 kJ/mol.H_2, exactly matching the value imposed by the DOE. On the other hand, a 25 % insertion of Si into the aluminum of Na_3AlH_6 results in a slight decrease in formation enthalpy to −56.58 kJ/mol.H_2. In contrast, a concentration of 50 % reduces the formation enthalpy of the $Na_3Al_{0.5}Si_{0.5}H_6$ system to −35.02 kJ/mol.H_2. In this same context, we observe that the enthalpy follows a linear decrease, and a concentration of 40 % Si could bring the enthalpy down to −40 kJ/mol.H_2, corresponding to the ideal value from the DOE [33,39,60]. Regarding iron, we find that the reaction enthalpy also follows a linear trend, reaching −50.99 kJ/mol.H_2 for a concentration of 50 %, indicating that the material remains more stable despite the high substitution concentration.

3.3.3. *Decomposition temperature*

The second thermodynamic factor to improve is the decomposition temperature T_d. According to the conditions set by the U.S. Department of Energy (DOE), the best hydride is one that operates under ambient conditions. For use in fuel cells (PEM), the temperature must be in the range of 289–393 K [20,51]. First, to calculate this temperature, we refer to Van't Hoff's law (Equation (9)) [35,57,61–63].

$$\Delta G = \Delta H - T_d \Delta S \tag{9}$$

With ΔG representing Gibbs energy, ΔH the formation enthalpy, T_d the decomposition temperature, and ΔS the entropy. At equilibrium, ΔG = 0 [22,30]. Since the entropy of the system depends on the thermal agitation of hydrogen atoms, most hydrides exhibit an entropy of ΔS ≈ 130 J/mol.K [10,64,65]. Therefore, the decomposition temperature can be determined using Equation (10).

$$T_d = \frac{\Delta H}{\Delta S} \tag{10}$$

The results show that Na_3AlH_6 hydride has a very high temperature of 632.76 K, which exceeds the operating range of fuel cells (PEM), which is 289–393 K [51,56]. Therefore, it is necessary to find a solution to make it compatible with this temperature range.

To do this, we recalculated the temperature of the substituted hydrides $Na_3Al_{1-x}M_xH_6$ (with x = 0.25 and 0.5 and M = Be, Si, and Fe). The results obtained are illustrated in Fig. 6, where the amber area corresponds to the temperature range of fuel cells. As shown in this fig, the decomposition temperature T_d decreases linearly with the increase in substitution percentage. Specifically, the temperature of the unsubstituted hydride is 632.76 K, while for the hydride substituted with 25 % Be ($Na_3Al_{0.75}Be_{0.25}H_6$), this temperature reaches 263.36 K. This is close to the temperature range of 289–393 K required for use in fuel cells (PEM) [20,22,51,60].

On the other hand, when the substitution reaches 50 % Be ($Na_3Al_{0.5}Be_{0.5}H_6$), the temperature drops to −9.47 K, a very low value compared to the operating range of fuel cells (PEM) [10,66]. These results clearly show that substituting aluminum with beryllium can meet the temperature requirements for fuel cells. For example, substituting aluminum with beryllium percentages between 18 % and 23 % could adjust the decomposition temperature within the range 289–393K required for fuel cells (PEM). For substitution with iron, the best result is obtained with a 50 % substitution of aluminum by iron ($Na_3Al_{0.5}Fe_{0.5}H_6$), which raises the temperature to 392.22 K, perfectly aligning with the operating range of fuel cells. In contrast, for the substitution of aluminum with silicon ($Na_3Al_{0.75}Si_{0.25}H_6$ and $Na_3Al_{0.5}Si_{0.5}H_6$), the obtained temperatures are 435.26 K and 269.39 K, respectively. As shown in Fig. 2, substitutions with percentages ranging from 33 % to 45 % allow for adjusting the temperature within the required range for fuel cells (PEM).

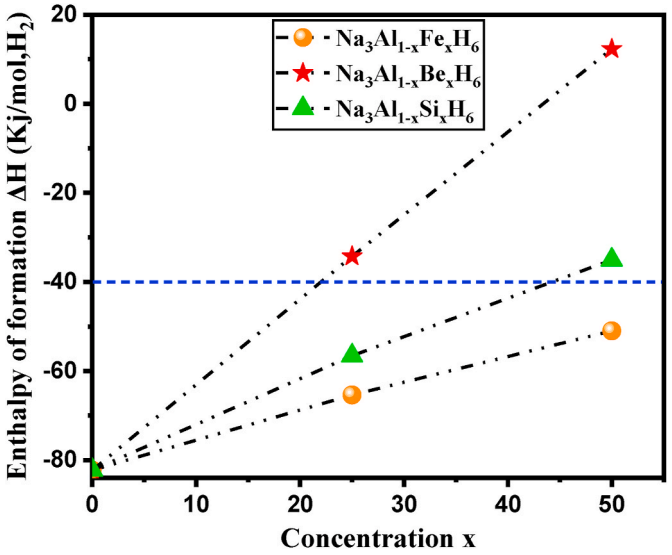

Fig. 5. Formation Enthalpy of Na_3AlH_6 and $Na_3Al_{1-x}M_xH_6$ (M = Be, Si, and Fe) with x = 0.25 and 0.5.

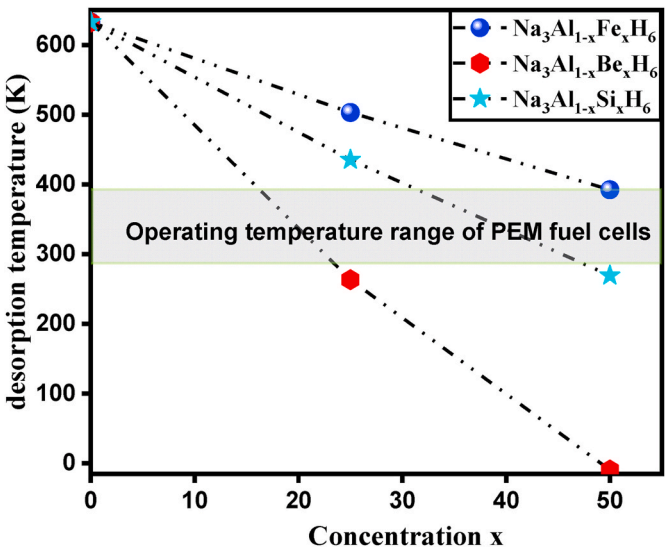

Fig. 6. Decomposition temperature T_d of Na_3AlH_6 and $Na_3Al_{1-x}M_xH_6$ (x = 0.25 and 0.5) (M = Be, Si, and Fe).

3.4. Density of states

To understand the electronic modifications occurring in Na_3AlH_6 hydride after substitution, it is therefore evident to compare the total (TDOS) and partial (PDOS) density of states of Na_3AlH_6 and $Na_3Al_{1-x}M_xH_6$ (with x = 0.25 and 0.5) and (M = Be, Si, and Fe) [35,39]. All analyses were conducted using the (GGA-PBEsol) approximation. The results obtained are illustrated in Fig. 7, where the dashed line corresponds to the Fermi level E_f and serves as a reference.

The analysis of the total density of states (TDOS) shows that Na_3AlH_6 hydride exhibits insulating characteristics, with a band gap of 2.98 eV, very close to the theoretical values of 3.9 eV [49], and 2.73 eV [67]. When aluminum is substituted by 25 % and 50 % of Be, Si, and Fe, this band gap is modified or shifted towards the valence band or the conduction band due to factors related to the atomic radii and electronegativity of the substituted elements.

More specifically, as shown in Fig. 7, when aluminum is replaced by silicon ($Na_3Al_{1-x}Si_xH_6$ with x = 0.25 and 0.5), the band gap shifts towards the valence band. This shift can be explained by the fact that silicon has a higher electronegativity compared to the other substituted elements, such as iron and beryllium, examined in this study. For substitution with iron ($Na_3Al_{1-x}Fe_xH_6$), the gap is slightly shifted towards the conduction band, and a decrease in the band gap is observed, reaching 2.6 eV for a substitution percentage of 25 % ($Na3Al_{0.75}Fe_{0.25}H_6$) and 2.7 eV for 50 % ($Na_3Al_{0.5}Fe_{0.5}H_6$). In the same way, for substitution with beryllium ($Na_3Al_{1-x}Be_xH_6$), a slight shift of the gap towards the conduction band and a slight decrease in the band gap are observed, with values of 2.76 eV for 25 % substitution ($Na_3Al_{0.75}Be_{0.25}H_6$) and 2.83 eV for 50 % ($Na_3Al_{0.5}Be_{0.5}H_6$).

On the other hand, the peaks of the total density of states (TDOS) vary with the substitution percentages, and this variation can explain the phenomena discussed earlier, particularly the structural and thermodynamic properties. For example, the conduction band peaks increase in the cases of ($Na_3Al_{0.75}Be_{0.25}H_6$), ($Na_3Al_{0.75}Si_{0.25}H_6$), and ($Na_3Al_{0.75}Fe_{0.25}H_6$), reaching 13.48, 12.80, and 13.61 states/eV, respectively, compared to the conduction band peak of Na_3AlH_6, which is 6.8 states/eV. In contrast, for ($Na_3Al_{0.5}Be_{0.5}H_6$) and ($Na_3Al_{0.5}Si_{0.5}H_6$), the peaks decrease slightly to 6.61 and 6.64 states/eV, respectively, while for ($Na_3Al_{0.5}Fe_{0.5}H_6$), there is a slight increase to 6.98 states/eV. This increase observed with iron substitution may be due to iron having a larger atomic radius than aluminum, which is reversed for substitutions with beryllium and silicon. A similar phenomenon is observed in the valence band. For instance, the peak of this band is 9.27 states/eV for the unsubstituted hydride Na_3AlH_6. For ($Na_3Al_{0.75}Be_{0.25}H_6$), ($Na_3Al_{0.75}Si_{0.25}H_6$), and ($Na_3Al_{0.75}Fe_{0.25}H_6$), this peak significantly increases to 18.10, 17.10, and 19.13 states/eV, respectively. In contrast, this peak decreases in the cases of ($Na_3Al_{0.5}Be_{0.5}H_6$) and ($Na_3Al_{0.5}Si_{0.5}H_6$), with values of 9.23 and 8.75 states/eV. However, there is a slight increase in the case of substitution with 50 % iron ($Na_3Al_{0.5}Fe_{0.5}H_6$), reaching 11.80 states/eV due to the atomic radius of iron.

4. Conclusion

In this work, we examined the influence of substituting aluminum (Al) in Na_3AlH_6 hydride with elements such as Be, Si, and Fe, at percentages of 25 % and 50 %. The results obtained show that:

- ✓ The substitution of aluminum with 25 % Be and 50 % Si results in enthalpies of −34.24 kJ/mol.H_2 and -35.02 kJ/mol.H_2, respectively. This is closer to the ideal value proposed by the DOE for selecting suitable materials for hydrogen storage.
- ✓ The substitution of aluminum with 50 % Fe results in a temperature of 392.22 K, which is required for materials used in fuel cells (PEM).
- ✓ The substitution of aluminum with 50 % Be increases the gravimetric capacity to 6.40 wt%, which meets the conditions proposed by the DOE.
- ✓ The substitution of aluminum with 50 % Fe increases the volumetric capacity to 47.2 g.H_2/L, which meets the standards proposed by the DOE.

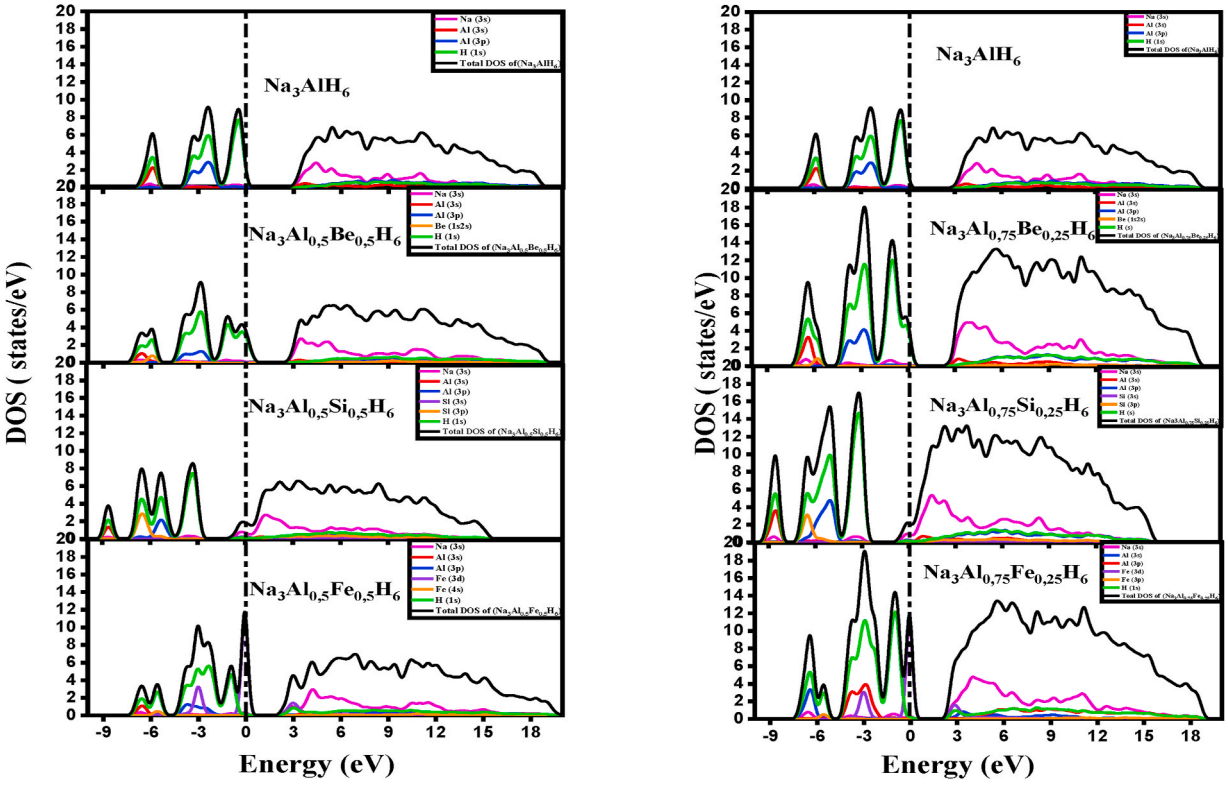

Fig. 7. PDOS and TDOS of Na_3AlH_6 and $Na_3Al_{1-x}M_xH_6$ (x = 0.25 and 0.5) (M = Be, Si, and Fe).

CRediT authorship contribution statement

Abdelmajid Assila: Writing – review & editing, Writing – original draft, Visualization, Supervision, Software, Resources, Methodology, Investigation, Data curation, Conceptualization. **Ikram Belkoufa:** Writing – review & editing, Resources. **Seddiq Sebbahi:** Writing – review & editing, Resources. **Amine Alaoui-Belghiti:** Visualization, Supervision, Methodology, Conceptualization. **El-kebir Hlil:** Writing – review & editing, Writing – original draft, Software, Resources, Methodology, Investigation, Conceptualization. **Mouhaydine Tlemçani:** Writing – review & editing, Writing – original draft, Methodology, Conceptualization. **Abdelowahed Hajjaji:** Writing – review & editing, Supervision, Resources, Formal analysis. **Said laasri:** Writing – original draft, Visualization, Resources, Methodology, Conceptualization.

Declaration of competing interest

The authors declare that they have no known competing financial interests or personal relationships that could have appeared to influence the work reported in this paper.

Data availability

No data was used for the research described in the article.

References

[1] A. Garratt, I. Petrella, Y. Zhang, Asymmetry and interdependence when evaluating U.S. Energy Information Administration forecasts, Energy Econ. 121 (2023) 106620, https://doi.org/10.1016/j.eneco.2023.106620.

[2] V. Rai, R. Tongia, G. Shrimali, N. Abhyankar, Data for development: the case for an Indian energy information administration, Energy Res. Social Sci. 25 (2017) 105–109, https://doi.org/10.1016/j.erss.2017.01.002.

[3] M. Luo, G. Jiang, M. Yu, Y. Yan, Z. Qin, Y. Li, Q. Zhang, Constructing crystalline homophase carbon nitride S-scheme heterojunctions for efficient photocatalytic hydrogen evolution, J. Mater. Sci. Technol. 161 (2023) 220–232, https://doi.org/10.1016/j.jmst.2023.03.038.

[4] J. Chen, Z. Li, H. Yu, X. Wang, Y. Xie, W. Zhou, Periodic quantum well mediated oriented charge separation in $Cd_{0.3}Zn_{0.7}S$ twin crystal towards optimized photocatalytic hydrogen evolution, Mater. Sci. Eng. R Rep. 161 (2024) 100843, https://doi.org/10.1016/j.mser.2024.100843.

[5] G. Şenol, F. Selimefendigil, H.F. Öztop, A review on nanofluid, phase change material and machine learning applications for thermal management of hydrogen storage in metal hydrides, Int. J. Hydrogen Energy 68 (2024) 1178–1208, https://doi.org/10.1016/j.ijhydene.2024.04.215.

[6] M.-K. Song, S. Park, F.M. Alamgir, J. Cho, M. Liu, Nanostructured electrodes for lithium-ion and lithium-air batteries: the latest developments, challenges, and perspectives, Mater. Sci. Eng. R Rep. 72 (2011) 203–252, https://doi.org/10.1016/j.mser.2011.06.001.

[7] J.B. Smith, S.H. Schneider, M. Oppenheimer, G.W. Yohe, W. Hare, M. D. Mastrandrea, A. Patwardhan, I. Burton, J. Corfee-Morlot, C.H.D. Magadza, H.-M. Füssel, A.B. Pittock, A. Rahman, A. Suarez, J.-P. Van Ypersele, Assessing dangerous climate change through an update of the Intergovernmental Panel on Climate Change (IPCC) "reasons for concern,", Proc. Natl. Acad. Sci. U.S.A. 106 (2009) 4133–4137, https://doi.org/10.1073/pnas.0812355106.

[8] R. Falkner, The Paris Agreement and the new logic of international climate politics, Int. Aff. 92 (2016) 1107–1125, https://doi.org/10.1111/1468-2346.12708.

[9] S. Matemilola, O. Fadeyi, T. Sijuade, Paris agreement, in: S. Idowu, R. Schmidpeter, N. Capaldi, L. Zu, M. Del Baldo, R. Abreu (Eds.), Encyclopedia of Sustainable Management, Springer International Publishing, Cham, 2020, pp. 1–5, https://doi.org/10.1007/978-3-030-02006-4_516-1.

[10] A. Assila, M. Rkhis, A. Alaoui-Belghiti, S. Laasri, E.K. Hlil, Y. Boughaleb, A. Hajjaji, Feeling the strain: enhancing the thermodynamics characteristics of magnesium nickel hydride Mg_2NiH_4 for hydrogen storage applications through strain engineering, Int. J. Hydrogen Energy 67 (2024) 651–657, https://doi.org/10.1016/j.ijhydene.2024.04.159.

[11] A. Allouhi, O. Zamzoum, M.R. Islam, R. Saidur, T. Kousksou, A. Jamil, A. Derouich, Evaluation of wind energy potential in Morocco's coastal regions, Renew. Sustain. Energy Rev. 72 (2017) 311–324, https://doi.org/10.1016/j.rser.2017.01.047.

[12] T. Da Silva Veras, T.S. Mozer, D. Da Costa Rubim Messeder Dos Santos, A. Da Silva César, Hydrogen: trends, production and characterization of the main process worldwide, Int. J. Hydrogen Energy 42 (2017) 2018–2033, https://doi.org/10.1016/j.ijhydene.2016.08.219.

[13] M. Ball, M. Weeda, The hydrogen economy – vision or reality? 1 1This paper is also published as Chapter 11 'The hydrogen economy – vision or reality?', in: Michael Ball, Angelo Basile, T. Nejat Veziroglu (Eds.), Compendium of Hydrogen Energy Volume 4: Hydrogen Use, Safety and the Hydrogen Economy, Elsevier, 2015 https://doi.org/10.1016/j.ijhydene.2015.04.032. ISBN: 978-1-78242-364-5. For further details see: http://www.elsevier.com/books/compendium-of-hydrogen-energy/ball/978-1-78242-364-5., International Journal of Hydrogen Energy 40 (2015) 7903–7919.

[14] R. Bridgeland, A. Chapman, B. McLellan, P. Sofronis, Y. Fujii, Challenges toward achieving a successful hydrogen economy in the US: potential end-use and infrastructure analysis to the year 2100, Clean. Prod. Lett 3 (2022) 100012, https://doi.org/10.1016/j.clpl.2022.100012.

[15] S. Rong, J. Ma, H. Zhang, J. Yu, T. Wang, Y. Cai, Z. Han, Y. Ji, Potential prediction in aqueous organic redox-targeting flow batteries: DFT calculation and experimental validation, Energy Storage Mater. 69 (2024) 103389, https://doi.org/10.1016/j.ensm.2024.103389.

[16] G. Zhang, J. Liu, S. Wei, F. Xu, L. Sun, Y. Xia, H. Wang, J. Wu, Y. Gao, Q. Shao, Y. Bu, Y. Guan, L. Liao, T. Liang, L. Qin, Thermally induced in situ fabrication of TiO_2/CN heterojunction dopant for enhancement of hydrogen storage properties of $LiAlH_4$, J. Mater. Sci. Technol. 203 (2024) 227–236, https://doi.org/10.1016/j.jmst.2024.02.067.

[17] Z. Abdin, A. Zafaranloo, A. Rafiee, W. Mérida, W. Lipiński, K.R. Khalilpour, Hydrogen as an energy vector, Renew. Sustain. Energy Rev. 120 (2020) 109620, https://doi.org/10.1016/j.rser.2019.109620.

[18] K. Müller, K. Brooks, T. Autrey, Releasing hydrogen at high pressures from liquid carriers: aspects for the H_2 delivery to fueling stations, Energy Fuel. 32 (2018) 10008–10015, https://doi.org/10.1021/acs.energyfuels.8b01724.

[19] E. Solomin, I. Kirpichnikova, R. Amerkhanov, D. Korobatov, M. Lutovats, A. Martyanov, Wind-hydrogen standalone uninterrupted power supply plant for all-climate application, Int. J. Hydrogen Energy 44 (2019) 3433–3449, https://doi.org/10.1016/j.ijhydene.2018.12.001.

[20] A. Assila, M. Rkhis, S. Sebbahi, A. Alaoui Belghiti, S. Laasri, E.K. Hlil, K. Zaidat, S. Obbade, A. Hajjaji, Improvement of the thermodynamic properties of lithium borohydride LiBH4 by mechanical treatment for hydrogen storage applications: a DFT investigation, Int. J. Hydrogen Energy 51 (2024) 72–78, https://doi.org/10.1016/j.ijhydene.2023.10.317.

[21] J.S. Shaikh, M. Rittiruam, T. Saelee, V. Márquez, N.S. Shaikh, P. Khajondetchairit, S. Pathan, P. Kanjanaboos, T. Taniike, M.K. Nazeeruddin, P. Praserthdam, S. Praserthdam, First-principles and experimental insight of high-entropy materials as electrocatalysts for energy-related applications: hydrogen evolution, oxygen evolution, and oxygen reduction reactions, Mater. Sci. Eng. R Rep. 160 (2024) 100813, https://doi.org/10.1016/j.mser.2024.100813.

[22] M. Rkhis, R. Anoua, A. Alaoui-Belghiti, S. Laasri, S. Touhtouh, E.K. Hlil, M. Bououdina, K. Zaidat, S. Obbade, A. Hajjaji, Role of vacancy defects on the dehydrogenation properties of the ternary hydride ZrNiH3: ab-initio insights, Int. J. Hydrogen Energy 46 (2021) 13088–13096, https://doi.org/10.1016/j.ijhydene.2021.01.100.

[23] M. Lakhal, M. Bhihi, H. Labrim, A. Benyoussef, S. Naji, A. Belhaj, B. Khalil, M. Abdellaoui, O. Mounkachi, M. Loulidi, A. El kenz, Kinetic Monte Carlo and density functional study of hydrogen diffusion in magnesium hydride MgH_2, Int. J. Hydrogen Energy 38 (2013) 8350–8356, https://doi.org/10.1016/j.ijhydene.2013.04.157.

[24] J. Zheng, X. Liu, P. Xu, P. Liu, Y. Zhao, J. Yang, Development of high pressure gaseous hydrogen storage technologies, Int. J. Hydrogen Energy 37 (2012) 1048–1057, https://doi.org/10.1016/j.ijhydene.2011.02.125.

[25] I. Eames, M. Austin, A. Wojcik, Injection of gaseous hydrogen into a natural gas pipeline, Int. J. Hydrogen Energy 47 (2022) 25745–25754, https://doi.org/10.1016/j.ijhydene.2022.05.300.

[26] R. Urbanczyk, K. Peinecke, M. Felderhoff, K. Hauschild, W. Kersten, S. Peil, D. Bathen, Aluminium alloy-based hydrogen storage tank operated with sodium aluminium hexahydride Na_3AlH_6, Int. J. Hydrogen Energy 39 (2014) 17118–17128, https://doi.org/10.1016/j.ijhydene.2014.08.101.

[27] R. Urbanczyk, K. Peinecke, M. Meggouh, P. Minne, S. Peil, D. Bathen, M. Felderhoff, Design and operation of an aluminium alloy tank using doped Na_3AlH_6 in kg scale for hydrogen storage, J. Power Sources 324 (2016) 589–597, https://doi.org/10.1016/j.jpowsour.2016.05.102.

[28] F.A. Halim Yap, M. Ismail, Functions of MgH_2 in the hydrogen storage properties of a Na_3AlH_6 - $LiBH_4$ composite, J. Phys. Chem. C 122 (2018) 23959–23967, https://doi.org/10.1021/acs.jpcc.8b07934.

[29] J. Huot, S. Boily, V. Güther, R. Schulz, Synthesis of Na_3AlH_6 and Na_2LiAlH_6 by mechanical alloying, J. Alloys Compd. 283 (1999) 304–306, https://doi.org/10.1016/S0925-8388(98)00875-5.

[30] W. Qian, Z. Chen, J. Zhang, L. Yin, Monolayer $MoSi_2N_4$ as promising electrocatalyst for hydrogen evolution reaction: a DFT prediction, J. Mater. Sci. Technol. 99 (2022) 215–222, https://doi.org/10.1016/j.jmst.2021.06.004.

[31] M. Rkhis, A. Alaoui-Belghiti, S. Laasri, S. Touhtouh, A. Hajjaji, E.K. Hlil, L. Bessais, D. Soubane, K. Zaidat, S. Obbade, First principal investigation on hydrogen solid storage in $Zr_{1-x}NbxNiH_3$ (x = 0 and 0.1), Int. J. Hydrogen Energy 44 (2019) 23188–23195, https://doi.org/10.1016/j.ijhydene.2019.07.017.

[32] J. Bellosta von Colbe, J.-R. Ares, J. Barale, M. Baricco, C. Buckley, G. Capurso, N. Gallandat, D.M. Grant, M.N. Guzik, I. Jacob, E.H. Jensen, T. Jensen, J. Jepsen, T. Klassen, M.V. Lototskyy, K. Manickam, A. Montone, J. Puszkiel, S. Sartori, D. A. Sheppard, A. Stuart, G. Walker, C.J. Webb, H. Yang, V. Yartys, A. Züttel, M. Dornheim, Application of hydrides in hydrogen storage and compression: achievements, outlook and perspectives, Int. J. Hydrogen Energy 44 (2019) 7780–7808, https://doi.org/10.1016/j.ijhydene.2019.01.104.

[33] L.E. Klebanoff, J.O. Keller, 5 Years of hydrogen storage research in the U.S. DOE metal hydride center of excellence (MHCoE), Int. J. Hydrogen Energy 38 (2013) 4533–4576, https://doi.org/10.1016/j.ijhydene.2013.01.051.

[34] S. Satyapal, J. Petrovic, C. Read, G. Thomas, G. Ordaz, The U.S. Department of energy's national hydrogen storage Project: progress towards meeting hydrogen-

powered vehicle requirements, Catal. Today 120 (2007) 246–256, https://doi.org/10.1016/j.cattod.2006.09.022.
[35] M. Rkhis, A. Alaoui-Belghiti, S. Laasri, S. Touhtouh, A. Hajjaji, E.K. Hlil, M. Bououdina, K. Zaidat, S. Obbade, Enhanced thermodynamic properties of $ZrNiH_3$ by substitution with transition metals (V, Ti, Fe, Mn and Cr), Int. J. Hydrogen Energy 45 (2020) 25002–25012, https://doi.org/10.1016/j.ijhydene.2020.06.213.
[36] M. Ismail, Y. Zhao, S.X. Dou, An investigation on the hydrogen storage properties and reaction mechanism of the destabilized MgH_2 - Na_3AlH_6 (4:1) system, Int. J. Hydrogen Energy 38 (2013) 1478–1483, https://doi.org/10.1016/j.ijhydene.2012.11.035.
[37] J. Zhang, D. Zhou, J. Liu, First-principles investigation of Mg_2CoH_5 complex hydride, Trans. Nonferrous Metals Soc. China 19 (2009) 205–209, https://doi.org/10.1016/S1003-6326(08)60253-8.
[38] I. Belkoufa, A. Assila, A. Alaoui-Belghiti, S. Laasri, E.K. Hlil, A. Hajjaji, Strain matters: Enhancing the hydrogenation properties of Mg_2CoH_5 through multiaxial approaches, Int. J. Hydrogen Energy 105 (2025) 1114–1122, https://doi.org/10.1016/j.ijhydene.2025.01.353.
[39] H. Benzidi, M. Lakhal, A. Benyoussef, M. Hamedoun, M. Loulidi, A. El kenz, O. Mounkachi, First principal study of strain effect on structural and dehydrogenation properties of complex hydride $LiBH_4$, Int. J. Hydrogen Energy 42 (2017) 19481–19486, https://doi.org/10.1016/j.ijhydene.2017.06.068.
[40] W. Lohstroh, A. Roth, H. Hahn, M. Fichtner, Thermodynamic effects in nanoscale $NaAlH_4$, ChemPhysChem 11 (2010) 789–792, https://doi.org/10.1002/cphc.200900767.
[41] B. Yebka, G.-A. Nazri, Synthesis and thermal characteristics of complex metal hydride: $NaAlH_4$, MRS Proc 801 (2003), https://doi.org/10.1557/PROC-801-BB4.4. BB4.4.
[42] B. Bogdanović, M. Schwickardi, Ti-doped alkali metal aluminium hydrides as potential novel reversible hydrogen storage materials, J. Alloys Compd. 253–254 (1997) 1–9, https://doi.org/10.1016/S0925-8388(96)03049-6.
[43] H. Yukawa, N. Morisaku, Y. Li, K. Komiya, R. Rong, Y. Shinzato, R. Sekine, M. Morinaga, Raman scattering and lattice stability of $NaAlH_4$ and Na_3AlH_6, J. Alloys Compd. 446–447 (2007) 242–247, https://doi.org/10.1016/j.jallcom.2007.02.071.
[44] H.Z. Yu, J.H. Dai, Y. Song, Catalytic effect of Ti on dehydrogenation of Na_3AlH_6: a first principles investigation, Int. J. Hydrogen Energy 40 (2015) 11478–11483, https://doi.org/10.1016/j.ijhydene.2015.01.156.
[45] C. Weidenthaler, A. Pommerin, M. Felderhoff, W. Schmidt, B. Bogdanović, F. Schüth, Evidence for the existence of β-Na_3AlH_6: monitoring the phase transformation from α-Na_3AlH_6 by in situ methods, J. Alloys Compd. 398 (2005) 228–234, https://doi.org/10.1016/j.jallcom.2005.02.021.
[46] E. Rönnebro, D. Noréus, K. Kadir, A. Reiser, B. Bogdanovic, Investigation of the perovskite related structures of $NaMgH_3$, $NaMgF_3$ and Na_3AlH_6, J. Alloys Compd. 299 (2000) 101–106, https://doi.org/10.1016/S0925-8388(99)00665-9.
[47] B. Bogdanovic, R.A. Brand, A. Marjanovic, M. Schwickardi, J. Tolle, Metal-doped sodium aluminium hydrides as potential new hydrogen storage materials, J. Alloys Compd. 302 (2000) 36–58, https://doi.org/10.1016/S0925-8388(99)00663-5.
[48] C. Qiu, S.M. Opalka, G.B. Olson, D.L. Anton, Thermodynamic modeling of the sodium alanates and the NaAlH system, Int. J. Mater. Res. 97 (2006) 1484–1494, https://doi.org/10.3139/146.101410.
[49] H. Oguchi, M. Matsuo, S. Kuromoto, H. Kuwano, S. Orimo, Sodium-ion conduction in complex hydrides $NaAlH_4$ and Na_3AlH_6, J. Appl. Phys. 111 (2012) 036102, https://doi.org/10.1063/1.3681362.
[50] V.P. Balema, L. Balema, Missing pieces of the puzzle or about some unresolved issues in solid state chemistry of alkali metal aluminohydrides, Present Address: 3917 Mendoci, Phys. Chem. Chem. Phys. 7 (2005) 1310, https://doi.org/10.1039/b419490j.
[51] M. Rkhis, S. Laasri, S. Touhtouh, E.K. Hlil, A. Hajjaji, Tailoring the electrochemical performance of olivine phosphate cathode materials for Li-ion batteries by strain engineering: computational experiments, ACS Appl. Energy Mater. (2023), https://doi.org/10.1021/acsaem.3c00711 acsaem.3c00711.
[52] M.J. Rutter, C2x: a tool for visualisation and input preparation for Castep and other electronic structure codes, Comput. Phys. Commun. 225 (2018) 174–179, https://doi.org/10.1016/j.cpc.2017.12.008.
[53] J.P. Perdew, K. Burke, M. Ernzerhof, Generalized gradient approximation made simple, Phys. Rev. Lett. 77 (1996) 3865–3868, https://doi.org/10.1103/PhysRevLett.77.3865.
[54] O. Sadek, S. Touhtouh, M. Rkhis, R. Anoua, M. El Jouad, F. Belhora, A. Hajjaji, Synthesis by sol-gel method and characterization of nano-TiO_2 powders, Mater. Today Proc. 66 (2022) 456–458, https://doi.org/10.1016/j.matpr.2022.06.385.
[55] M. Rkhis, A. Alaoui-Belghiti, S. Laasri, S. Touhtouh, E.K. Hlil, M. Bououdina, K. Zaidat, S. Obbade, A. Hajjaji, Dependence of Mg, Be and Al substitution on the hydrogen storage characteristics of $ZrNiH_3$, Int. J. Energy Res. 45 (2021) 2292–2302, https://doi.org/10.1002/er.5922.
[56] M. Rkhis, S. Laasri, S. Touhtouh, E.K. Hlil, M. Bououdina, R. Ahuja, K. Zaidat, S. Obbade, A. Hajjaji, Engineering the hydrogen storage properties of the perovskite hydride $ZrNiH_3$ by uniaxial/biaxial strain, Int. J. Hydrogen Energy 47 (2022) 3022–3032, https://doi.org/10.1016/j.ijhydene.2021.10.237.
[57] I. Belkoufa, B. Misski, A. Alaoui-Belghiti, M. Mouyane, D. Houivet, S. Laasri, E. K. Hlil, A. Hajjaji, Role of Mg, Ca, and Mo in $NaBH_4$ systems for hydrogen storage applications: ab initio study, Comput. Mater. Sci. 242 (2024) 113090, https://doi.org/10.1016/j.commatsci.2024.113090.
[58] J.G.O. Ojwang, R. Van Santen, G. Jan Kramer, X. Ke, An ab initio study of possible pathways in the thermal decomposition of $NaAlH_4$, J. Solid State Chem. 181 (2008) 3037–3043, https://doi.org/10.1016/j.jssc.2008.08.010.
[59] B.-M. Lee, J.-W. Jang, J.-H. Shim, Y.W. Cho, B.-J. Lee, Thermodynamic assessment of the $NaH \leftrightarrow Na_3AlH_6 \leftrightarrow NaAlH_4$ hydride system, J. Alloys Compd. 424 (2006) 370–375, https://doi.org/10.1016/j.jallcom.2006.01.008.
[60] I. Belkoufa, B. Misski, A. Alaoui-Belghiti, C. Moslah, M. Mouyane, D. Houivet, S. Laasri, E.K. Hlil, A. Hajjaji, Improved thermodynamic properties of (Sc, V, Ti, Fe, Mn, Co, and Ni) doped $NaBH_4$ for hydrogen storage: first-principal calculation, Int. J. Hydrogen Energy 68 (2024) 481–490, https://doi.org/10.1016/j.ijhydene.2024.04.155.
[61] S. Akrami, P. Edalati, M. Fuji, K. Edalati, High-entropy ceramics: review of principles, production and applications, Mater. Sci. Eng. R Rep. 146 (2021) 100644, https://doi.org/10.1016/j.mser.2021.100644.
[62] E.H. Majzoub, E.C.E. Rönnebro, Methodology of materials discovery in complex metal hydrides using experimental and computational tools, Mater. Sci. Eng. R Rep. 73 (2012) 15–26, https://doi.org/10.1016/j.mser.2012.01.001.
[63] J. Zhu, X. Lin, L. Lv, M. Li, Q. Luo, V.N. Kudiiarov, W. Liu, H. Leng, X. Han, Z. Ma, The relationship between thermal management methods and hydrogen storage performance of the metal hydride tank, J. Mater. Sci. Technol. 203 (2024) 66–77, https://doi.org/10.1016/j.jmst.2024.03.018.
[64] B. Ahmed, M.B. Tahir, A. Ali, M. Sagir, First-principles screening of structural, electronic, optical and elastic properties of Cu-based hydrides-perovskites $XCuH_3$ (X=Ca and Sr) for hydrogen storage applications, Int. J. Hydrogen Energy 54 (2024) 1001–1007, https://doi.org/10.1016/j.ijhydene.2023.11.239.
[65] J. Graetz, Y. Lee, J.J. Reilly, S. Park, T. Vogt, Structure and thermodynamics of the mixed alkali alanates, Phys. Rev. B 71 (2005) 184115, https://doi.org/10.1103/PhysRevB.71.184115.
[66] M. Rkhis, S. Laasri, S. Touhtouh, E.K. Hlil, K. Zaidat, S. Obbade, A. Hajjaji, New insights into the electrochemical and thermodynamic properties of AB-type ZrNi hydrogen storage alloys by native defects and H-doping: computational experiments, Int. J. Hydrogen Energy (2022) S0360319922058311, https://doi.org/10.1016/j.ijhydene.2022.12.115.
[67] X. Ke, I. Tanaka, Decomposition reactions for $NaAlH_4$, Na_3AlH_6, and NaH: first-principles study, Phys. Rev. B 71 (2005) 024117, https://doi.org/10.1103/PhysRevB.71.024117.